Solid-State NMR and Quantum Chemical Investigations of $^{13}C^\alpha$ Shielding Tensor Magnitudes and Orientations in Peptides: Determining ϕ and ψ Torsion Angles

Sungsool Wi,[†] Haihong Sun,[‡] Eric Oldfield,*,[‡,§] and Mei Hong*,[†]

Contribution from the Department of Chemistry, Iowa State University, Gilman Hall 0108, Ames, Iowa 50011, and the Departments of Biophysics and Chemistry, University of Illinois at Urbana-Champaign, 600 South Mathews Avenue, Urbana, Illinois 61801

Received November 23, 2004; E-mail: mhong@iastate.edu

Abstract: We report the experimental determination of the $^{13}C^\alpha$ chemical shift tensors of Ala, Leu, Val, Phe, and Met in a number of polycrystalline peptides with known X-ray or de novo solid-state NMR structures. The 700 Hz dipolar coupling between $^{13}C^\alpha$ and its directly bonded ^{14}N permits extraction of both the magnitude and the orientation of the shielding tensor with respect to the $C^\alpha-N$ bond vector. The chemical shift anisotropy (CSA) is recoupled under magic-angle spinning using the SUPER technique (Liu et al., *J. Magn. Reson.* **2002**, *155*, 15−28) to yield quasi-static chemical shift powder patterns. The tensor orientation is extracted from the $^{13}C-^{14}N$ dipolar modulation of the powder line shapes. The magnitudes and orientations of the experimental $^{13}C^\alpha$ chemical shift tensors are found to be in good accord with those predicted from quantum chemical calculations. Using these principal values and orientations, supplemented with previously measured tensor orientations from $^{13}C-^{15}N$ and $^{13}C-^{1}H$ dipolar experiments, we are able to predict the (ϕ, ψ, χ_1) angles of Ala and Val within 5.8° of the crystallographic values. This opens up a route to accurate determination of torsion angles in proteins based on shielding tensor magnitude and orientation information using labeled compounds, as well as the structure elucidation of noncrystalline organic compounds using natural abundance ^{13}C NMR techniques.

Introduction

There is currently considerable interest in the use of chemical shifts to probe the structures of proteins, both in solution and in the crystalline solid state. Isotropic chemical shifts of $^{13}C^\alpha$, $^{13}C^\beta$, and $^{1}H^\alpha$ have been studied most extensively and have been found to be strong functions of secondary structure.[2] When supplemented with ^{15}N, $^{13}C'$, and H^N chemical shifts, these isotropic shifts have been quite successful in predicting peptide backbone torsion angles (ϕ, ψ), using a database approach.[3] Another approach to predicting peptide backbone structure makes use of the relationships between chemical shift tensor and structure, which can be obtained from quantum chemical calculations.[4,5] In such calculations, both the principal values of the shielding tensors as well as their orientations are obtained, all of which can in principle be used to determine structure. For example, information on the magnitudes of the $^{13}C^\alpha$ shielding tensor in an Ala-containing tripeptide has been used to predict (ϕ, ψ) values to within ~10° of a crystallographic

value.[6] However, the use of CSA principal values alone tend to generate multiple solutions for (ϕ, ψ), and it is likely that additional information, on tensor *orientations*, may be valuable for reducing the number of possible solutions, as well as for increasing their accuracy.

To illustrate the dependence of the C^α shielding tensor orientation on protein secondary structure, we summarize in Figure 1 the calculated C^α tensor orientations (from http://feh.scs.uiuc.edu) for 18 amino acids (excluding Gly and Pro) in their most populous side chain conformations. The tensor orientation is expressed by the polar angle β and the azimuthal angle α of the $C^\alpha-N$ bond (a) and the $C^\alpha-H^\alpha$ bond (b) with respect to the *z*-principal axis of the chemical shift tensor, which is defined as the one furthest from the isotropic shift. Discernible trends and correlations can be seen between the (ϕ, ψ) torsion angles and the tensor orientation (α, β). For example, for parallel β-sheet structures ($\phi = -120°$, $\psi = 120°$), the orientation of the C^α tensor relative to the $C-N$ bond (green circles in Figure 1a) clusters in regions of large (α, β). For helical structures ($\phi = -60°$, $\psi = -45°$), α and β exhibit a large range and appear to be anti-correlated, as shown by the black square symbols and dotted ellipse in Figure 1a. For the helical residues, the C^α shift tensor orientation also depends on the nature of the side chain. For example, the β-branched residues Ile and Val have

---

† Iowa State University.
‡ Department of Biophysics, University of Illinois at Urbana-Champaign.
§ Department of Chemistry, University of Illinois at Urbana-Champaign.
(1) Liu, S. F.; Mao, J. D.; Schmidt-Rohr, K. *J. Magn. Reson.* **2002**, *155*, 15−28.
(2) Wishart, D. S.; Sykes, B. D.; Richards, F. M. *J. Mol. Biol.* **1991**, *222*, 311−333.
(3) Cornilescu, G.; Delaglio, F.; Bax, A. *J. Biomol. NMR* **1999**, *13*, 289−302.
(4) deDios, A. C.; Pearson, J. G.; Oldfield, E. *Science* **1993**, *260*, 1491−1496.
(5) Sitkoff, D.; Case, D. A. *Prog. Nucl. Magn. Reson. Spectrosc.* **1998**, *32*, 165−190.

---

(6) Havlin, R. H.; Laws, D. D.; Bitter, H. L.; Sanders, L. K.; Sun, H.; Grimley, J. S.; Wemmer, D. E.; Pines, A.; Oldfield, E. *J. Am. Chem. Soc.* **2001**, *123*, 10362−10369.
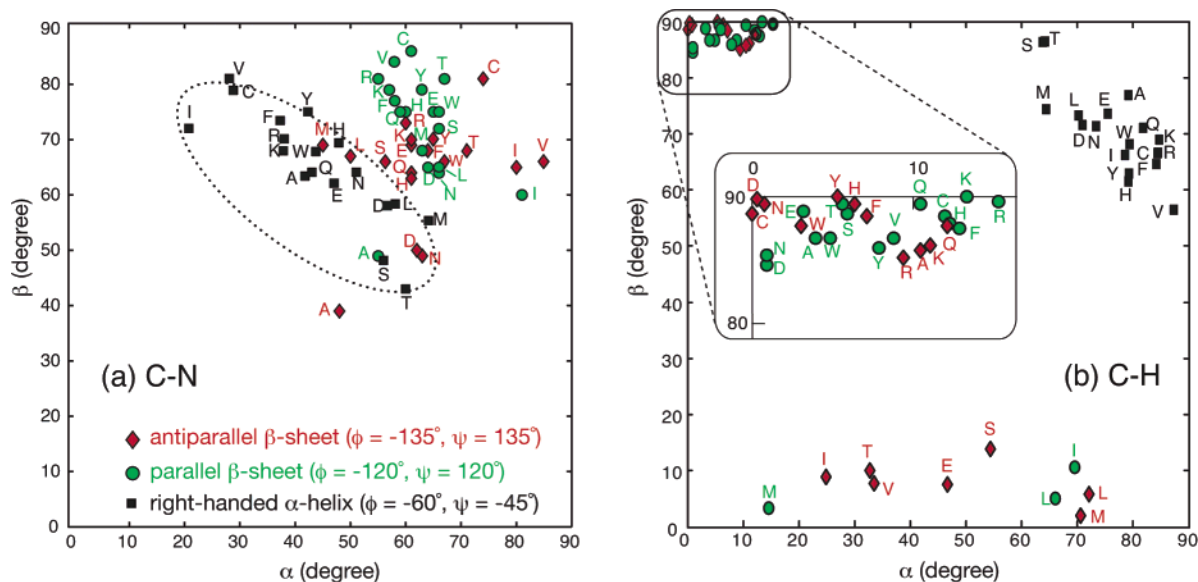
Figure 1. Dependence of C^α shielding tensor orientations on secondary structure and amino acid type. Antiparallel β sheet (red ◆, $\phi = -135°$, $\psi = 135°$), parallel β-sheet (green ●, $\phi = -120°$, $\psi = 120°$), and right-handed α-helix (black ■, $\phi = -60°$, $\psi = -45°$). (a) The polar (β) and azimuthal (α) angles of the $C^\alpha-N$ bond vector relative to the $^{13}C^\alpha$ shielding tensor for different amino acids. (b) The polar (β) and azimuthal (α) angles of the $C^\alpha-H^\alpha$ bond vector relative to the $^{13}C^\alpha$ shielding tensor.

large β and small α, while the OH-containing residues, Ser and Thr, have large α and small β. All four aromatic amino acids (Phe, Tyr, Trp and His) cluster, as do all residues having extended aliphatic side chains (Met, Leu, Asp, Asn, Glu, Gln, Arg, and Lys).

The orientation of the C^α shielding tensor relative to the $C^\alpha-H^\alpha$ bond vector also shows dramatic clustering and dependence on (ϕ, ψ) angles (Figure 1b). Helical residues exhibit large α and β, while β-sheet residues are clustered in two regions, one with high β and low α, the other with low β values. The results shown in Figure 1 indicate that C^α shielding tensor orientations vary considerably with backbone torsion angles[7] as well as with amino acid type. Since the shielding surfaces for all amino acids are now available,[8] Figure 1 suggests the possibility of deducing (ϕ, ψ) values for amino acids in proteins, based on experimentally measured (α, β) values and tensor magnitude.

While the principal components of the chemical shift tensor can be measured readily with sideband techniques such as 2D PASS[9] and FIREMAT,[10] the orientation of the C^α chemical shift tensor in a molecular segment requires more involved techniques. Experimental determination of chemical shielding tensor orientations thus far has mostly utilized single-crystal NMR. We recently introduced an approach that allows the determination of shielding tensor orientation from powder samples under magic-angle spinning (MAS). This approach relies on dipolar modulation of the C^α anisotropic chemical shift line shape by $^{13}C^\alpha-^{15}N$ and $^{13}C^\alpha-^1H^\alpha$ dipolar couplings.[11] The CSA powder pattern is recoupled under MAS using the SUPER sequence,[1] while the $^{13}C-^{15}N$ or $^{13}C-^1H$ dipolar couplings are suitably recoupled to modulate the CSA line shape.[11,12] In

contrast to sideband-based techniques, this approach produces CSA powder patterns in the indirect dimension of the 2D spectra that resemble the static spectra.

In the absence of the ^{15}N label, the naturally abundant (99.6%) ^{14}N spin, a quadrupolar nucleus with a spin quantum number $I = 1$, dipolar-couples to the $^{13}C^\alpha$ spin with a strength of ~0.7 kHz (corresponding to a $C^\alpha-N$ bond length of 1.46 Å). At the moderate magnetic field strength of 9.4 T, this $^{13}C^\alpha-^{14}N$ coupling produces characteristic and observable modulation on the recoupled C^α powder patterns. The quasi-static CSA line shapes can then be simulated to extract the principal values as well as the principal axis orientation relative to the C–N bond.[13] Applying the experiment to several peptides, we find that the experimental CSA principal values agree with the calculated values to an average of 2.4 ppm, while the difference in the tensor orientation is less than 14°. Moreover, we show that by combining various tensor orientation restraints from independent experiments, we can accurately predict the backbone torsion angles ϕ and ψ (and for Val, χ_1) in peptides. This opens up the possibility of carrying out related experiments on proteins by using ^{13}C-labeled samples.

Materials and Methods

Sample Preparation. The natural abundance peptides Gly-Ala-Phe (GAF), Gly-Ala-Leu (GAL), and Gly-Gly-Val (GGV) were purchased from Bachem (Torrance, CA). *N*-Formyl-Met-Leu-Phe (f-MLF) and *N*-acetyl-Val (NAV) were purchased from the American Peptide Company (Sunnyvale, CA) and Sigma (St. Louis, MO), respectively. All samples were used without further purification. 2-Propanol solutions of f-MLF and GAF and aqueous solutions of GAL and NAV were used to recrystallize the samples. The crystal structures of GAF and GAL were directly determined by single-crystal X-ray diffraction and found to be identical to the literature structures.[14,15] For NAV, the literature X-ray structure[16,17] was used for the quantum chemical

(7) Walling, A. E.; Pargas, R. E.; deDios, A. C. *J. Phys. Chem. A* **1997**, *101*, 7299−7303.
(8) Sun, H.; Sanders, L. K.; Oldfield, E. *J. Am. Chem. Soc.* **2002**, *124*, 5486−5495.
(9) Antzutkin, O. N.; Lee, Y. K.; Levitt, M. H. *J. Magn. Reson.* **1998**, *135*, 144−155.
(10) Alderman, D. W.; McGeorge, G.; Hu, J. Z.; Pugmire, R.; Grant, D. M. *Mol. Phys.* **1998**, *95*, 1113−1126.
(11) Yao, X.; Hong, M. *J. Am. Chem. Soc.* **2002**, *124*, 2730−2738.
(12) Yao, X.; Yamaguchi, S.; Hong, M. *J. Biomol. NMR* **2002**, *24*, 51−62.

(13) Strohmeier, M.; Grant, D. M. *J. Am. Chem. Soc.* **2004**, *126*, 966−977.
(14) Ramasubbu, N.; Parthasarathy, R. *Biopolymers* **1989**, *28*, 1259−1269.
(15) Chaturvedi, S.; Go, K.; Parthasarathy, R. *Biopolymers* **1991**, *31*, 397−407.
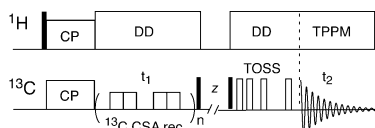
Figure 2. Pulse sequence for recoupling the $^{13}C^\alpha$ chemical shielding tensor with the $^{13}C^\alpha-^{14}N$ dipolar interaction in unlabeled peptides. This is equivalent to the original SUPER sequence[1]. No ^{14}N or ^{15}N decoupling is applied. DD: dipolar decoupling. TOSS: total sideband suppression.[19] TPPM: two-pulse phase modulation.[21]

calculations. For f-MLF, the de novo solid-state NMR structure[18] was used, since its X-ray structure is unavailable. The f-MLF ^{13}C chemical shifts we find are identical to those reported in the literature, indicating that the previously determined torsion angles are applicable to the present sample.

NMR Experiments. All NMR measurements were performed on a Bruker (Karlsruhe, Germany) DSX-400 spectrometer operating at 9.4 T, using a 4-mm double-resonance MAS probe. The pulse sequence for recoupling the $^{13}C^\alpha$ CSA and the $^{13}C^\alpha-^{14}N$ dipolar interaction under MAS is shown in Figure 2.[1] The 2D indirect time domain t_1 incorporates a phase-compensated 2π pulse train synchronized with the spinning speed, $\omega_r/2\pi$, of 2.5 kHz. To obtain the quasi-static CSA line shapes, we placed the 2π pulses symmetrically within the rotor period to remove the sine-modulated terms of the chemical shift frequency. The 2π pulses are placed at timings calculated such that the coefficients of the cosine modulated terms are proportional to the static anisotropic chemical shift[1] with a scaling factor of 0.155. Thus, the effective t_1 dwell time was set to t_r (nominal dwell time) $\times$ 0.155 = 62 μs, to give the unscaled magnitude of the CSA.[1] At the relatively slow spinning speed used, TOSS[19] and γ-angle averaging[20] were used to obtain centerband-only spectra in the direct dimension. The signal-averaging times for the 2D experiments were 8-22 h, depending on the recycle delay (1.5-3 s) and the number of scans (128 or 256). Gaussian line broadening of 40-100 Hz was applied in both dimensions of the 2D spectra. In all experiments, ^1H TPPM decoupling at ~70 kHz was applied during detection[21] and CW decoupling at ~90 kHz was applied during the t_1 period. The $^1H-^{13}C$ cross polarization (CP) contact time was 500 μs.

Conventions for CSA Magnitude and Orientation. The magnitude of the experimentally measured CSA was expressed as $\delta = \delta_{zz} - \delta_{iso}$ and $\eta = (\delta_{yy} - \delta_{xx})/\delta$, where $|\delta_{zz} - \delta_{iso}| \geq |\delta_{xx} - \delta_{iso}| \geq |\delta_{yy} - \delta_{iso}|$ and $\delta_{iso} = (\delta_{xx} + \delta_{yy} + \delta_{zz})/3$. This representation was used in spectral simulations. The experimental chemical shifts were referenced externally to the $^{13}C'$ signal of α-Gly at 176.4 ppm. The $(\delta_{xx}, \delta_{yy}, \delta_{zz})$ convention is convertible with the $(\delta_{11}, \delta_{22}, \delta_{33})$ convention. The latter corresponds to the least shielded, the intermediate shielded, and the most shielded chemical shifts, respectively $(\delta_{11} \geq \delta_{22} \geq \delta_{33})$.[22] The larger value of $|\delta_{11} - \delta_{iso}|$ or $|\delta_{33} - \delta_{iso}|$ becomes δ_{zz}, while the smaller value becomes δ_{xx}. The quantum chemical calculations yielded chemical shielding tensor parameters, σ_{ii} (i = 1, 2, or 3). The δ_{ii} and σ_{ii} (i = 1, 2, or 3) are matched in the indices. Since $\sigma_{11} \leq \sigma_{22} \leq \sigma_{33}$, we convert the traceless part of the shielding tensor, $\sigma_{iso} - \sigma_{ii}$, where $\sigma_{iso} = (\sigma_{11} + \sigma_{22} + \sigma_{33})/3$, to the shifts, $\delta_{ii} - \delta_{iso}$. To emphasize the spread of the CSA, we also use the span, $\Omega = \delta_{11} - \delta_{33} = \sigma_{33} - \sigma_{11}$.

The orientation of the $^{13}C^\alpha-^{14}N$ dipolar vector was expressed in the principal axis system $(\delta_{xx}, \delta_{yy}, \delta_{zz})$ of the $^{13}C^\alpha$ chemical shift tensor, using the polar angle β and the azimuthal angle α. The experimental

(16) Carroll, P. J.; Stewart, P. L.; Opella, S. J. *Acta Crystallogr.* **1990**, *C46*, 243-246.
(17) Lalitha, V.; Subramanian, E.; Bordner, J. *Int. J. Pept. Protein Res.* **1984**, *24*, 437-441.
(18) Rienstra, C. M.; Tucker-Kellogg, L.; Jaroniec, C. P.; Howhy, M.; Reif, B.; McMahon, M. T.; Tidor, B.; Lozano-Pérez, T.; Griffin, R. G. *Proc. Natl. Acad. Sci. U.S.A.* **2002**, *99*, 10260-10265.
(19) Dixon, W. T. *J. Chem. Phys.* **1982**, *77*, 1800-1809.
(20) deAzevedo, E. R.; Bonagamba, T. J.; Hu, W.; Schmidt-Rohr, K. *J. Chem. Phys.* **2000**, *112*, 8988-9001.
(21) Bennett, A. E.; Rienstra, C. M.; Auger, M.; Lakshmi, K. V.; Griffin, R. G. *J. Chem. Phys.* **1995**, *103*, 6951-6958.
(22) Jameson, C. J. *Solid State NMR* **1998**, *11*, 265-268.

Figure 3. Representative $^{13}C^\alpha$ CSA powder patterns (a-c) and isotropic (d-f) ^{13}C MAS NMR spectra of (a) Met in f-MLF, (b) Val in GGV, and (c) Leu in GAL. Note the ^{14}N modulation of the powder pattern, especially in (b).
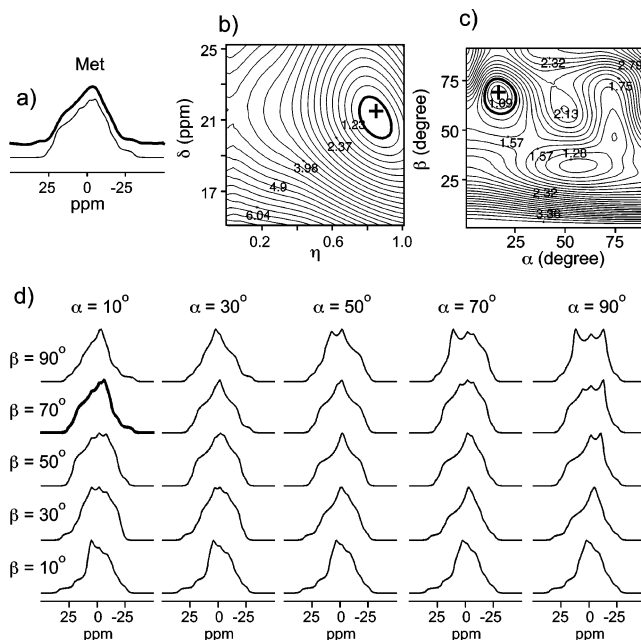
Figure 4. Met C^α CSA. (a) Experimental (top, in bold) and best-fit (bottom) CSA spectra. (b) 2D RMSD plot as a function of δ and η. (c) 2D RMSD plot as a function of (α, β) between the shielding tensor and the $C^\alpha-N$ vector. All RMSD values are normalized by the minimum RMSD value. (d) Simulated $^{13}C-^{14}N$ modulated C^α CSA spectra for various (α, β) angles. The near best-fit spectrum is shown in bold.

CSA spectra were simulated first to obtain the principal values (δ_{xx}, δ_{yy}, δ_{zz}), then to obtain the tensor orientations in terms of (α, β) with respect to the δ_{zz} axis. The angles α and β span from 0 to 2π and from 0 to π, respectively. Because of the degenerate conditions $\beta \equiv \pi - \beta$ and $\alpha \equiv \pi \pm \alpha \equiv 2\pi - \alpha$, we considered only the range $0 \leq (\alpha, \beta) \leq \pi/2$ in the simulations.

Since ab initio calculated tensor orientations were expressed as direction cosines β_{ii} between σ_{ii} (i = 1, 2, 3) and the $C^\alpha-N$ vector, we converted the (α, β) angles from the experimental best fits to the direction cosines according to:[12]

$$\cos \beta_{zz} = \cos \beta$$

$$\cos \beta_{xx} = \sin \beta \cos \alpha$$

$$\cos \beta_{yy} = \sin \beta \cos \alpha \tag{1}$$

Table 1. Summary of $^{13}C^\alpha$ shielding tensors from experiment and ab initio calculations[a]

	M in f-MLF		L in f-MLF		A in GAF		F in GAF	
	expt	calcd	expt	calcd	expt	calcd	expt	calcd
ϕ (deg)	−146	−150	−89.5	−90	−71.6	−75.0	−78.4	−78
ψ (deg)	159	165	−39.5	−45	−33.4	−30.0	−42.9	−43
χ_1 (deg)	−85	−65.0	−58.7	−60			−77.8	−78
Ω (ppm)	41 ± 3	42.2	42.5 ± 2.0	34.4	34.4 ± 1.9	33.4	38.9 ± 3.0	29.0
η	0.85 ± 0.05	0.89	0.40 ± 0.05	0.34	0.7 ± 0.1	0.69	0.7 ± 0.1	0.64
δ_{iso} (ppm)[b]	51.2		56.7		53.5		61.5	
$\delta_{11}-\delta_{iso}$ (ppm)[b]	21.3 ± 1.0	21.7	17.5 ± 1.3	13.6	15.8 ± 1.4	14.8	17.9 ± 2.0	15.8
$\delta_{22}-\delta_{iso}$ (ppm)[b]	−1.6 ± 0.7	−1.2	7.5 ± 0.8	6.7	2.8 ± 0.8	3.7	3.2 ± 1.0	4.6
$\delta_{33}-\delta_{iso}$ (ppm)[b]	−19.7 ± 1.7	−20.5	−25.0 ± 1.0	−20.4	−18.6 ± 0.5	−18.6	−21.0 ± 1.0	−20.4
β_{11} (deg)[c]	70 ± 5	70	47 ± 20	82	117 ± 15	107	51 ± 15	41
β_{22} (deg)[c]	104 ± 5	114	135 ± 20	149	33 ± 15	51	41 ± 15	56
β_{33} (deg)[c]	25 ± 5	32	103 ± 10	120	108 ± 10	136	80 ± 10	71

	A in GAL		L in GAL		V in GGV		V in NAV	
	expt	calcd	expt	calcd	expt	calcd	expt	calcd
ϕ (deg)	−65.7	−60	−72.2	−75.0	-81.5	−81.5	−137	−135
ψ (deg)	−40	−45	−45.3	−45.0	129	129	178	180
χ_1 (deg)			−68.5	−60.0	180	180	−60	−60
Ω (ppm)	36.0 ± 1.0	29.9	39.4 ± 3.0	33.1	25.0 ± 2.5	22.9	46.6 ± 3.1	42.4
η	0.89 ± 0.05	0.92	0.53 ± 0.1	0.47	0.33 ± 0.1	0.99	0.68 ± 0.1	0.53
δ_{iso} (ppm)[b]	52.0		57.2		65.3		57.3	
$\delta_{11}-\delta_{iso}$ (ppm)[b]	17.5 ± 1.0	15.2	17.1 ± 2.0	14.0	10.0 ± 1.5	11.4	25.3 ± 1.0	24.0
$\delta_{22}-\delta_{iso}$ (ppm)[b]	1.0 ± 0.6	−0.7	5.2 ± 1.3	5.1	5.0 ± 1.1	0.1	−4.0 ± 1.5	−5.6
$\delta_{33}-\delta_{iso}$ (ppm)[b]	−18.5 ± 1.0	−14.7	−22.3 ± 1.0	−19.1	−15.0 ± 1.0	−11.5	−21.3 ± 2.1	−18.3
β_{11} (deg)[c]	131 ± 15	117	54 ± 20	69.4	59 ± 25	64	67 ± 20	66.6
β_{22} (deg)[c]	50 ± 15	53.5	135 ± 20	142	32 ± 25	26	141 ± 25	139
β_{33} (deg)[c]	67 ± 10	48.4	67 ± 10	59.4	99 ± 10	93.3	60 ± 25	58.5

[a] The calculational results were made using *N*-formyl-X-amide fragments and the most populous sidechain geometries and are available on line at http://feh.scs.uiuc.edu. [b] Experimental chemical shifts δ_{ii} are referenced to the C′ isotropic shift of Gly at 176.4 ppm on the TMS scale. [c] β_{ii} is the angle between the C^α−N bond vector and δ_{ii} (σ_{ii}).

β_{yy} is always equal to β_{22}, while β_{zz} equals β_{33} or β_{11}, depending on which principal component is farthest from the isotropic shift.

Computational Aspects. The $^{13}C^\alpha$ shielding tensor magnitudes and orientations were taken from previously reported[9] results (http://feh.scs.uiuc.edu), which were obtained using the Hartree−Fock method with a uniform 6-311++G(2d,2p) basis on AMBER force-field geometry-optimized *N*-formyl-X-amide models.[4,8] Since these published results are primarily for the most populous side chain conformers, we also carried out a new set of calculations employing the actual side chain geometries of each peptide. These results are provided in the Supporting Information.

Results and Discussion

We show in Figure 3a−c the recoupled C^α chemical shift powder spectra (in the traceless representation) of *MLF, GG*V, and GA*L (the asterisk before the single-letter amino acid code denotes the residue of interest), extracted from the indirect dimension of the 2D SUPER spectra. The corresponding 1D CP-MAS spectra of the peptides are shown in Figure 3d−f. The isotropic line widths of these samples are very narrow (∼0.4 ppm), indicating conformational homogeneity. The effects of the $^{13}C-^{14}N$ dipolar couplings are seen as additional modulations at the top of the powder patterns. The ^{14}N nucleus splits the two $|\pm1/2\rangle$ eigenstates of the $^{13}C^\alpha$ nucleus into three eigenstates in the $^{13}C-^{14}N$ coupled space, $|+1, \pm1/2\rangle$, $|0, \pm1/2\rangle$ and $|-1, \pm1/2\rangle$. This gives rise to three orientation-dependent powder line shapes. The sum of these three line shapes depends not only on the magnitudes of the $^{13}C^\alpha$ CSA and $^{13}C-^{14}N$ dipolar coupling, but also on their relative orientations.[13] Similarly, the isotropic ^{13}C spectra (d−f) also exhibit the influence of ^{14}N coupling, but as a splitting of 2:1 intensity ratio in the $^{13}C^\alpha$ signals. This results from higher-order quadrupole−

dipole cross-correlation:[23] the intensities of 2 and 1 correspond to the $|\pm1\rangle$ and $|0\rangle$ eigenstates of ^{14}N, respectively. Since this effect is much smaller than the CSA and the first-order dipolar couplings, it was not included in the simulations of the anisotropic CSA powder patterns.

We illustrate the extraction of the $^{13}C^\alpha$ CSA principal values and principal-axes orientations using the *MLF spectrum (Figure 4). The recoupled and $^{13}C-^{14}N$ modulated C^α CSA spectrum of Met (Figure 4a, bold) is shown together with its best-fit simulation (a, thin line). The best-fit simulation was obtained by minimizing the root mean square deviation (RMSD) between the experimental and simulated spectra. The anisotropy and asymmetry parameters (δ, η) were fitted first, and then the orientation angles (α, β) were optimized. About ∼8−10 iterations of magnitude and orientation optimization were performed to determine the best fit. Optimization of (δ, η) determines the breadth and shape of the powder pattern, while optimization of (α, β) determines the fine structure due to $^{13}C^\alpha-$ ^{14}N dipolar modulation. The RMSD between the experiment and simulations as a function of (δ, η) and (α, β) are shown in Figure 4b and c, respectively. The contour maps were generated by incrementing δ in steps of 0.2 ppm, η in steps of 0.02, and α and β in steps of 1°. The RMSD values were normalized to the best-fit RMSD value, which is represented by the cross. The bold contour lines represent the uncertainty of the best fits, which is estimated by comparing the experimental spectrum with simulated spectra of increasing angles away from the best fit until a significant difference is detected. To illustrate the sensitivity of the powder line shape to the $^{13}C-^{14}N$ dipolar

(23) Harris, R. K.; Oliveri, A. C. *Prog. Nucl. Magn. Reson. Spectrosc.* **1992**, *24*, 436−456.
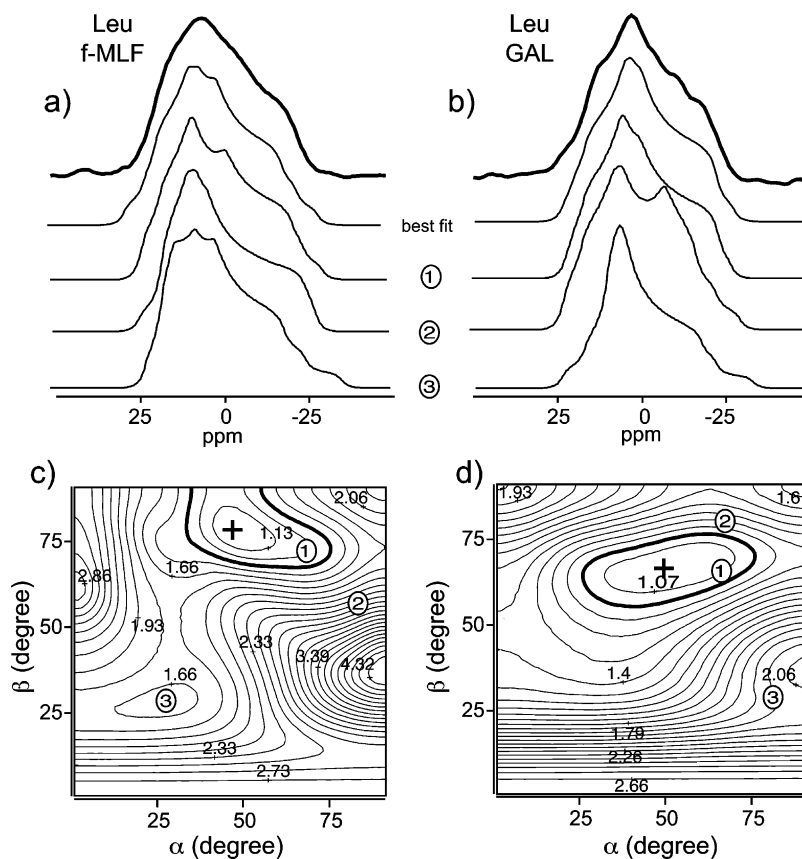
Figure 5. Leu ^{13}C$^\alpha$ spectra in f-MLF and GAL. (a) Experimental (bold), best-fit (+ in (c) and other simulated spectra (numbers in (c)) of Leu in f-MLF. (b) Same as that for (a), but of Leu in GAL. (c) 2D RMSD plot of C$^\alpha$ f-M*LF as a function of (α, β). (d) 2D RMSD plot of GA*L as a function of (α, β). The estimated experimental uncertainties in (α, β) are represented by bold contour lines.

coupling, we also show a panel of simulated spectra as a function of α and β in 20° steps (Figure 4d). It can be seen that both the width and the fine structure are affected by the tensor orientation. The Met C$^\alpha$ tensor orientation is one of the more difficult ones to extract among the peptides studied, since the CSA is large. With smaller CSAs, the effect of the ^{13}C$-^{14}$N dipolar modulation is more pronounced. The best-fit Met ^{13}C$^\alpha$ spectrum yields traceless principal values of $\delta_{11} - \delta_{iso} = 21.3 \pm 1.0$ ppm, $\delta_{22} - \delta_{iso} = -1.6 \pm 0.7$ ppm, and $\delta_{33} - \delta_{iso} = -19.7 \pm 1.7$ ppm, and the angles with the C$-$N bond are $\beta_{11} = 70° \pm 5°$, $\beta_{22} = 104° \pm 5°$, and $\beta_{33} = 25° \pm 5°$ (Table 1). Ab initio calculations for similar (ϕ, ψ) angles and with a standard side chain conformation ($\chi_1 = -65°$, $\chi_2 = -65°$, $\chi_3 = -70°$) yielded traceless principal values of (21.7, -1.2, -20.5) ppm and orientation angles of (70°, 114°, 32°), in good agreement with the experimental data (Table 1).

We next investigated the C$^\alpha$ CSAs of two Leu residues with α-helical torsion angles, in f-M*LF and GA*L. Parts a and b of Figure 5 show the recoupled CSA powder patterns (in bold), their best-fit simulations, and several simulated spectra with randomly chosen orientations (Figure 5, parts c and d). For (α, β) angles far away from the region of the best fit, the ^{13}C$-^{14}$N modulated line shapes deviate significantly from the experimental spectra. The orientational RMSD plots for the two residues (Figures 5, parts c and d) indicate angular uncertainties of $\pm 10°$ for β and $\pm 20°$ for α. The best-fit tensor elements and angles are compared with the ab initio calculations in Table 1. For both Leu residues, the calculated C$^\alpha$ CSA spans (33$-$34 ppm) are a factor of $\sim$0.82 of the measured CSA spans (39$-$

42 ppm), consistent with the Leu C$^\alpha$ CSAs reported for other model peptides.[6] The orientation angles deviate by 18°, on average, but are clearly largest for M*LF (24°), which may be associated with the use of an NMR (as opposed to an X-ray) derived structure.

The Val C$^\alpha$ CSAs in two peptides, NAV ($\phi = -137°$, $\psi = 178°$, $\chi_1 = -57°$) and GGV ($\phi = -81.5°$, $\psi = 129°$, $\chi_1 = 180°$), are shown in Figure 6. The main structural difference is the χ_1 angle, while the backbone torsion angles are loosely associated with the β-sheet region of the Ramachandran diagram. The recoupled CSA spectra do, however, show a dramatic difference in span (Figure 6a,b): 25.0 ppm (ab initio: 22.9 ppm) in GGV, but a much larger 46.6 ppm (ab initio: 42.4 ppm) in NAV. The best-fit spectra yield principal values and principal axes orientations that are in excellent agreement with the calculated results. The RMS deviation is 2.9 ppm in magnitude and 4.1° in orientational angles. The current ^{14}N-modulated spectra also agree well with previous ^{15}N-modulated CSA data.[11,12] The average magnitude and angle differences are 0.25 ppm and 2.7°, respectively, confirming the accuracy of the ^{14}N-modulation technique for extracting CSAs.

In the previous ^{15}N-modulated CSA experiment for GG*V,[12] we were concerned about an apparent inconsistency between the calculated and the experimental tensor axis orientation. Specifically, the calculated σ_{11} and σ_{22} components appeared to be swapped with respect to the experimental result. It now appears that this was the result of using the ψ_2 torsion angle ($-50.7°$) from the crystal structure, which referred to the double-bond O rather than the single-bond O. With the correct ψ_1
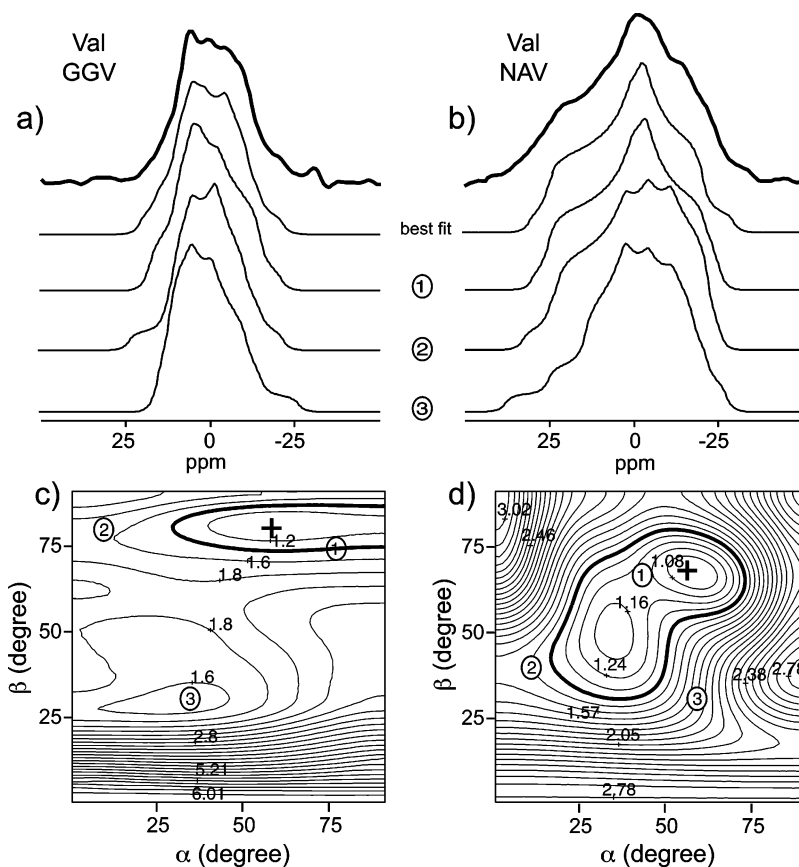
Figure 6. Val $^{13}C^\alpha$ spectra of (a) GGV and (b) NAV. Experimental (bold), best-fit, and other simulated spectra are shown. (c and d) 2D RMSD plot of GG*V and NA*V as a function of (α, β) angles.

torsion angle of 129°, the calculated principal axes orientations are completely consistent with the experiment (Table 1).

Experimental spectra and simulations for Phe in GA*F and Ala residues in G*AF and G*AL are compiled in the Supporting Information. For Phe (Figure S1), the best fit to the experimental spectrum yielded principal values of (17.9, 3.2, −21.0) ppm and orientation angles of (51°, 41°, 80°). The ab initio calculation differs from the experiment by an average of only 1.5 ppm and 12° (Table 1). For both Ala residues (Figure S2), which have helical torsion angles and similar CSA spans of ∼35 ppm, calculated tensor values deviate by 2.0 ppm from the experiment, while the calculated tensor orientations deviate by 17° from the experiment.

When the experimental shift and orientation results for all residues are plotted against the ab initio values, we find for the shifts a slope of 0.90, R^2 of 0.98, and an RMSD of 2.4 ppm, and for the orientational angles, a slope of 0.96, R^2 of 0.87, and an RMSD of 13.6° (Figure 7). To assess if there were noticeable improvements in the experiment/theory correlation by using the exact side chain geometries determined from X-ray or de novo NMR structures, we carried out alternative calculations using the same basic molecular fragment as described above, but setting the side chain torsion angles to the exact values reported. The resulting full tensor magnitudes and orientations are given in Table S1, and the theory/experiment comparison is shown in Figure S3. For the shifts, use of exact geometries yields a slope of 0.87, R^2 of 0.98, and an RMSD of 2.3 ppm. For the orientations, a slope of 0.89, R^2 of 0.72, and an RMSD of 20° are obtained. The differences between the two
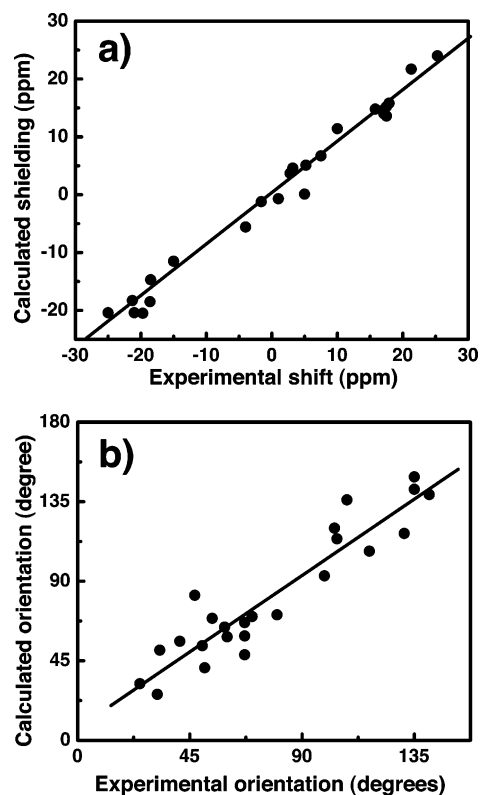
Figure 7. Comparisons between the experimental and calculated C^α chemical shift tensors for the peptides studied here. (a) Magnitude correlation: slope = 0.90, R^2 = 0.98, RMSD = 2.4 ppm. (b) Orientations correlation: slope = 0.96, R^2 = 0.87, RMSD = 13.6°.
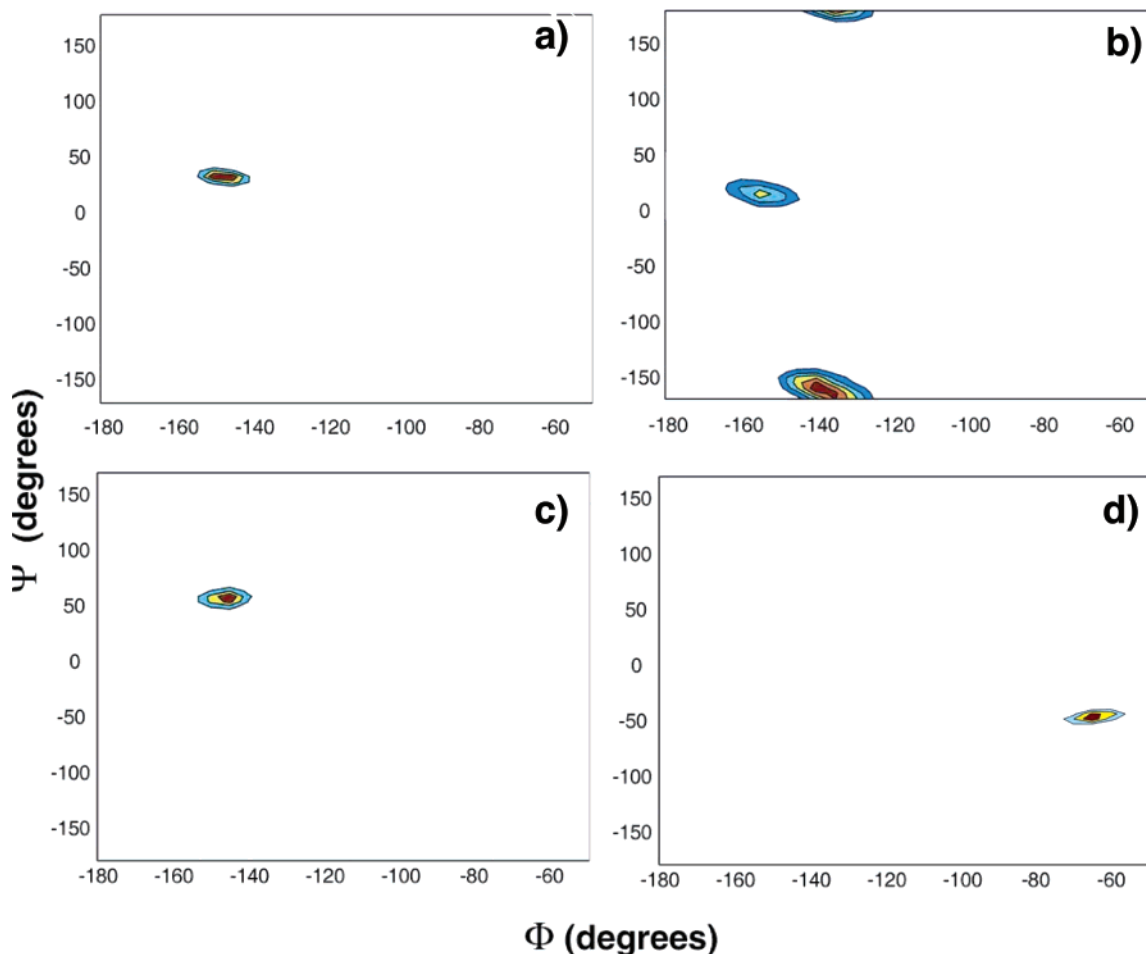
Figure 8. Z-Surface results for Val in NAV and Ala in GAL. (a) NAV, ^7Z, $\chi_1 = 180°$; (b) NAV, ^7Z, $\chi_1 = -60°$; (c) NAV, ^7Z, $\chi_1 = 60°$. The Z-surface parameters for (a–c) are: Ω (^{14}N), $\delta_{22} - \delta_{iso}$(^{14}N), β_{22} (^{14}N), Ω(^{15}N), $\delta_{22} - \delta_{iso}$(^{15}N), α_{11}(^{15}N), and β_{22}(^{15}N). (d) GAL ^{13}Z-surface, using experimental parameters of Ω(^{14}N), $\delta_{22} - \delta_{iso}$(^{14}N), β_{22}(^{14}N), Ω(^{15}N), $\delta_{22} - \delta_{iso}$(^{15}N), α_{11}(^{15}N), β_{22}(^{15}N), β_{11}(^{14}N), β_{33}(^{14}N), α_{22}(^{15}N), α_{33}(^{15}N), β_{11}(^{15}N), and β_{33}(^{15}N). All ^{15}N experimental data are from ref 12.

sets of calculations are small, consistent with the idea that (ϕ,ψ) angles dominate C^α shielding. The question then arises: are the results described above sufficiently accurate to be used for structure prediction?

To address this question, we use the Z-surface approach.[24] The idea behind the Z-surface method is to first compute a series of property surfaces, $P(\phi,\psi)$, then to compute the probability that a given value of a property, such as the span Ω or β_{22}, for a specific (ϕ, ψ) set, is consistent with the experimentally measured value. The probability is defined as:

$$Z = \exp\{-[P_{expt} - P(\phi,\psi)]^2/W\}$$

where P is the value of the property, such as Ω and β_{22}, and W is a search-width parameter. The most likely solution is the one that has the largest Z-value. The W values used were: $W = 3$ ppm for Ω, 1.5 ppm for $\delta_{22} - \delta_{iso}$, and 15° for β_{ii}. The W value for the span is essentially the same as before (2.58 ppm[25]), that for β_{ii} is close to the RMSD of β_{ii}, while the 1.5 ppm value for $\delta_{22} - \delta_{iso}$ was chosen to be half that of $\Omega = \delta_{33} - \delta_{11}$ surfaces, since there is essentially no error on the experimental δ_{iso}.

(24) Le, H. B.; Pearson, J. G.; deDios, A. C.; Oldfield, E. *J. Am. Chem. Soc.* **1995**, *117*, 3800–3807.
(25) Heller, J.; Laws, D. D.; Tomaselli, M.; King, D. S.; Wemmer, D. E.; Pines, A.; Havlin, R. H.; Oldfield, E. *J. Am. Chem. Soc.* **1997**, *119*, 7827–7831.

Table 2. *Z-Surface and Energy Results for NAV and GAL*

	χ_1	solution (ϕ, ψ)	Z	relative MM energy (kcal)
NA*V $(^7Z)^a$	180	−149, 30	2.8×10^{-10}	9.78
	−60	−140, −170	0.562	0
	60	−145, 65	2.77×10^{-4}	2.98
G*AL $(^7Z)^a$	NA	−65, 145	0.0194	0
	NA	−60.5, −38	0.002	0.03
G*AL $(^{13}Z)^b$	NA	−65, −38	0.00004	0

[a] The experimental properties used to generate the ^7Z-surface were Ω (^{14}N), $\delta_{22} - \delta_{iso}$(^{14}N), β_{22}(^{14}N), Ω(^{15}N), $\delta_{22} - \delta_{iso}$(^{15}N), α_{11}(^{15}N), and β_{22}(^{15}N). The ^{15}N experimental data are from refs 11 and 12. *[b]* To generate the ^{13}Z-surface, six additional restraints were added: α_{11}(^{15}N), α_{22}(^{15}N), α_{33}(^{15}N), β_{11}(^{15}N), β_{22}(^{15}N), and β_{33}(^{15}N). The ^{15}N experimental data are from ref 12.

We consider first the case of Val in NAV, in which we make no a priori assumptions about the side chain conformation. This necessitates the evaluation of three separate Z-surfaces, associated with the three possible lowest-energy χ_1 conformations. For $\chi_1 = 180°$, a ^7Z-surface is plotted in Figure 8a, using experimental restraints Ω(^{14}N), $\delta_{22} - \delta_{iso}$(^{14}N), β_{22}(^{14}N), Ω-(^{15}N), $\delta_{22} - \delta_{iso}$(^{15}N), α_{11}(^{15}N), and β_{22}(^{15}N), where α_{11} is the angle of the δ_{11} axis to the C–H vector measured previously.[12] A solution with $(\phi = -149°, \psi = 30°)$ was found, but has the very low Z-value of 2.8×10^{-10} (Table 2), an unlikely solution. For the $\chi_1 = -60°$ ^7Z-surface (Figure 8b), the solution is $(\phi =$

Table 3. Comparison of NMR Chemical-Shift Predicted Torsion Angles in Two Peptides with X-ray Values

peptide	NMR (ϕ, ψ, χ_1)	X-ray (ϕ, ψ, χ_1)
NA*V	(−140°, −170°, −60°)	(−137°, 178°, −57°)
G*AL	(−65°, −38°)	(−65.7°, −40°)
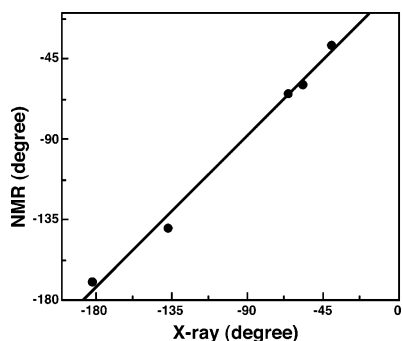
Figure 9. Correlation of the torsion angles deduced by X-ray and NMR (see Table 3).

−140°, ψ = −170°) with a much higher Z-value of 0.562. Indeed, this is very close to the X-ray value of (ϕ = −137°, ψ = 178°). A second solution can also be seen in Figure 8b, but it has a lower Z-value (0.12). For the χ_1 = 60° surface, ϕ = −145° and ψ = 65°, but Z = 2.8 × 10^{-4}, again a low value. The Z-values thus select the correct χ_1 value, −60°, for NAV and predict the (ϕ, ψ) torsion angles to within 3° and 12° of the X-ray structure.[16] Further support for this χ_1 assignment is obtained by considering the molecular mechanics (MM) energies of the major solutions, an approach we used previously.[26] As shown in Table 2, the χ_1 = −60° structure with ϕ = −140°, ψ = −170° has the lowest energy, consistent with its large Z-value.

Finally, we consider the case of Ala in GAL (Figure 8d), the only "central" residue in our tripeptides with an extensive amount of tensor data. The results of a ^{7}Z-surface yielded two possible solutions, but on addition of further orientational constraints reported previously, specifically $\alpha_{11}(^{15}N)$, $\alpha_{22}(^{15}N)$, $\alpha_{33}(^{15}N)$, $\beta_{11}(^{15}N)$, $\beta_{22}(^{15}N)$, and $\beta_{33}(^{15}N)$, we obtained a single ^{13}Z-surface solution (Figure 8d). This predicts the most likely torsion angles to be (ϕ = −65°, ψ = −38°) (Table 3), in excellent agreement with the crystal structure (ϕ = −65.7°, ψ = −40°).[15] The computed and crystallographic results for ϕ, ψ in NAV and GAL and for χ_1 in NAV are shown in Figure 9 and have an RMSD of 5.8°.

Taken together, these results suggest that the combined use of C$^\alpha$ shift tensor magnitude and orientation restraints should enable good predictions of ϕ and ψ torsion angles in peptides and, via isotopic labeling, in proteins, where tensor magnitude determinations have already been reported.[27]

Conclusion

The results shown above represent the first broad experimental survey of the magnitudes and the orientations of the C$^\alpha$ chemical shielding tensor in peptides. We find that both the magnitudes and the orientations of the principal components of the C$^\alpha$ shielding tensors are in good agreement with the results of ab initio calculations: a 2.4 ppm error on δ_{ii} and <14° on the tensor orientations. We used these experimental results in a Z-surface approach to see to what extent the backbone torsion angles ϕ and ψ can be predicted, making use of the structure ↔ spectra correlations reported previously.[7] For NA*V, both Z-surface and energetic considerations yielded a highly likely (ϕ, ψ, χ_1) structure close to the X-ray value. In the case of G*AL, two low-energy solutions were found in a ^{7}Z-surface but incorporation of additional tensor data resulted in selection of the correct (ϕ, ψ) solution with an average 1.5° deviation from the X-ray solution. Clearly, the use of multiple restraints for both tensor magnitudes and orientations, when combined with the Z-surface approach (or the related χ^2 approach[13]), can give very good (ϕ, ψ) predictions as well as information on χ_1. The use of both tensor magnitude[27] and orientation information therefore appears to be a promising approach to the determination of torsion angles in peptides and (with isotopic labeling) in proteins. It should also be of use for investigating the structures of noncrystalline proteins, such as highly ordered amyloid fibrils.[28]

Supporting Information Available: Computed tensor magnitudes and orientations obtained by using exact side chain geometries, experimental spectra of Phe in GAF and Ala in GAF and GAL, correlation between experimental and calculated chemical shift tensor magnitudes, and orientations using exact side chain geometries. This material is available free of charge via the Internet at http://pubs.acs.org.

JA042935B

(26) Pearson, J. G.; Le, H.; Sanders, L. K.; Godbout, N.; Havlin, R. H.; Oldfield, E. *J. Am. Chem. Soc.* **1997**, *119*, 11941−11950.

(27) Rienstra, C. M. Presented at the 45th Experimental NMR Conference, Asilomar, CA, 2004.
(28) Heise, H. et al. Presented at the 45th Experimental NMR Conference, Asilomar, CA, 2004.